On the origin and excitation of the extended nebula surrounding NGC 1275

N. A. Hatch,[⋆] C. S. Crawford, R. M. Johnstone and A. C. Fabian
Institute of Astronomy, Madingley Road, Cambridge, CB3 0HA

5 February 2008

ABSTRACT
We use line-of-sight velocity information on the filamentary emission-line nebula of NGC 1275 to infer a dynamical model of the nebula's flow through the surrounding intracluster gas. We detect outflowing gas and flow patterns that match simulations of buoyantly rising bubbles from which we deduce that some of the nebula filaments have been drawn out of NGC 1275. We find a radial gradient of the ratio [NII]λ6584/Hα which may be due to a variation in metallicity, interactions with the surrounding intracluster medium or a hardening of the excitation mechanism. We find no preferred spatial correlation of stellar clusters within the filaments and there is a notable lack of [OIII]λ5007 emission, therefore it is unlikely that the filaments are ionized by stellar UV.

Key words: galaxies: clusters: individual: Perseus - cooling flows - galaxies: individual: NGC 1275 - intergalactic medium.

1 INTRODUCTION

NGC 1275 is the central galaxy of the X-ray luminous Perseus cluster (A426), which has bright centrally peaked X-ray emission, and a cool core with a central temperature of a third the virial temperature (Schmidt et al. 2002; Sanders et al. 2004). Cavities in the X-ray emission are observed in a number of locations surrounding the central galaxy (Fabian et al. 2003a). Where these coincide with GHz radio emission they are interpreted as bubbles filled with relativistic plasma, which has been injected into the intracluster medium (ICM) by the central engine. Cavities with no observed radio emission have been described as 'ghost bubbles', and are thought to have originated from an earlier epoch of activity in the central engine.

Minkowski (1957) discovered that the nebula of NGC 1275 comprises of two distinct emission-line systems: a high-velocity system (8200 km s^{-1}), identified as a disrupted foreground galaxy (Boroson 1990) at least 60 kpc in front of NGC 1275 (Gillmon et al. 2004), and a low-velocity system (5265 km s^{-1}). Although the high-velocity system lies directly in front of NGC 1275, the emission lines are easily distinguished in wavelength from those of the low-velocity system, and clearly indicate photoionization by hot, young stars (Kent & Sargent 1979).

The low-velocity system associated with the central galaxy NGC 1275 is the focus of this work. It is known to extend over 100 kpc in a large array of thin filaments (Lynds 1970; Conselice et al. 2001). Whilst the nebula is extremely luminous– 4.1×10^{42} erg s^{-1} in Hα and [NII] (Heckman et al. 1989), with a total line luminosity probably 20 times that in Hα– the power

source remains unknown. Ionization by the central active galactic nucleus (AGN) residing in NGC 1275 can be ruled out as the dominant source of power for the extended nebula on the grounds that the Hα luminosity does not decrease with distance from the nucleus (Johnstone & Fabian 1988), although it may be important in the luminous inner regions. Ionization by hot young stars is an attractive option as it is a local mechanism, but the line ratios are drastically different to those seen in HII regions (Kent & Sargent 1979). Models of heating by X-rays from the ICM have been put forward (Donahue & Voit 1991), as well as conduction from the ICM (Donahue et al. 2000), shocks (Sabra et al. 2000) and turbulent mixing layers (Crawford & Fabian 1992).

Soft X-ray emission is associated with some of the optical filaments of NGC 1275 (Fabian et al. 2003b). The filaments are less luminous in the X-ray than the optical/UV by up to two orders of magnitude implying they are not excited by X-radiation. The soft X-ray emission indicates an interaction between the warm filaments and the hot ICM, possibly via heat conduction.

Large deposits of molecular hydrogen have been discovered in the central regions of NGC 1275 (Krabbe et al. 2000; Donahue et al. 2000) similar to other central cluster galaxies with emission-line nebulae (Edge et al. 2002). Recently, molecular hydrogen was observed in the outer filaments of NGC 1275 (Hatch et al. 2005), indicating gas at 2000 K exists within the hot ICM at radii of over 25 kpc.

The origin of the filaments remain a mystery. Current theories include condensing gas from the ICM in the form of a cooling flow (Fabian et al. 1984; Heckman et al. 1989; Donahue & Voit 1991), gas accreting from previous mergers (Braine et al. 1995), the explosive expulsion of gas from NGC 1275 (Burbidge & Burbidge 1965) or gas drawn out (Fabian et al. 2003b). The filaments are very thin,

⋆ E-mail:nah@ast.cam.ac.uk

long and the majority are radial. Submerged within the ICM, they enable us to constrain the level of turbulence in the ICM and argue for a laminar flow. As the ICM moves it may drag the warm optically emitting gas, thus the filaments can act as streamlines tracing the flow direction(Fabian et al. 2003b).

None of these problems are exclusive to NGC 1275 as extended emission-line nebulae are commonly found surrounding other massive galaxies in the centre of X-ray bright 'cool cores', where the X-ray emission is centrally peaked (Crawford et al. 1999).

This work presents new spectroscopic data that explore the kinematic and line-emission properties of the nebula that surrounds NGC 1275. After analysing and interpreting the kinematics we put forward a dynamical model of the nebula and discuss the origin of the filaments. The redshift of NGC 1275 is 0.0176, which using $H_0 = 70 \, \mathrm{km \, s^{-1} Mpc^{-1}}$, gives 1 kpc$\simeq$2.7 arcsec.

2 OBSERVATIONS AND DATA REDUCTION

The data were obtained on the nights of 2004 Sept 23 and 2004 Oct 06 using the GMOS North instrument on the Gemini North telescope on Mauna Kea, Hawaii. The sky on both nights was photometric and the seeing was less than 0.8 arcsec. Six slit positions were chosen using the map of Conselice et al. (2001; see Fig 1), selected to feature particular structures of interest. Two bright stars were aligned on each slit so its exact position was known. The slit width was 0.5 arcsec, filter R831+G590 was used and the exposure time for each slit was 900 seconds (3×300s); all exposures were binned 2×2 before readout. This setup allows us to explore the observed wavelength range 4850–6945Å. The spectroscopic standards BD+28d4211 and G1912B2 were observed in order to flux-calibrate the data. A flat was taken with the GCAL instrument after every slit position observed. CuAr arcs and bias frames were taken with the GCAL instrument on the nights of the 2004 Sept 23 and 2004 Oct 05. A summary of all science exposures taken is given in Table 1.

The data were reduced using the IRAF Gemini package (version 1.7). The bias frames were combined, flatfields were normalised and mosaiced together. All science and standard star frames were reduced by bias subtraction, mosaicing the individual chips together, flatfielding and interpolating across the detector gaps. The arcs were calibrated and checked manually against a line list before the wavelength solution was transferred to the data. The science observations were flux calibrated using the standard star G1912B2 (BD+28d4211 was not used as it was observed 35° from the parallactic angle and showed signs of strong atmospheric differential refraction), and finally sky-subtracted. The data were de-reddened for Galactic extinction using E(B–V)=0.315. The spectra were extracted, converted to ASCII format and analysis was performed using QDP (Tennant 1990). The red section covering [OI]λ6300 to [SII]λ6731 was fitted separately to a blue section covering the lines of Hβ to [NI]λ5199. The HeI 5876 was fitted separately. The lines were assumed to be Gaussian in profile and share the same redshift and velocity width. [NII]λ6548 was assumed to have a third of the intensity of the [NII]λ6584 line.

Acquisition images were taken at all slit positions through the r G0303 filter. These images were reduced by bias subtraction, flatfielding, then normalised and combined using the IRAF IMAGES package to form an *R*-band image with a scale of 0.1454 arcsec/pixel. The image was used to accurately align the slits with the Hα image from Conselice et al. (2001).

Position	Exposure type	Filter	Exposure time (sec)
Slit 1	Spectral	R831+G590	900
Slit 1	Image	rG0303	100
Slit 2	Spectral	R831+G590	900
Slit 3	Spectral	R831+G590	900
Slit 3	Image	rG0303	60
Slit 4	Spectral	R831+G590	900
Slit 4	Image	rG0303	300
Slit 5	Spectral	R831+G590	900
Slit 5	Image	rG0303	80
Slit 6	Spectral	R831+G590	900
Slit 6	Image	rG0303	300

Table 1. Summery of Gemini observations.

Figure 1 details all six longslit positions. Slit 1 cuts through the Northern filaments. Slit 2 covers the top of the 'horseshoe' feature to the Northwest and cuts through the main Northern filament. Slit 3 covers the short straight radial western part of the 'horseshoe' feature and cuts across the North-East of the nebula. Slit 4 covers the long 30 kpc radial filament that runs from the galaxy into the 'horseshoe' loop on the Eastern side. Slit 5 runs along the North of the nebula covering a long tangential filament. Slit 6 covers the dominant Northern filament and passes through the Western side of the nebula.

3 ARCHIVAL HST DATA

We extracted archival Hubble Space Telescope WFPC2 imaging data on NGC 1275 in three broad bands: F450W (with total exposure time of 5100 s), F702W (4700 s) and F814W (4800 s). At the redshift of NGC 1275, the strong emission lines of Hα+[NII] (from the low-velocity system only) appear in the F702W bandpass.

4 STELLAR CLUSTERS AND CONTINUUM

NGC 1275 is surrounded by many star clusters (Holtzman et al. 1992; Carlson et al. 1998), which are clearly visible strewn across the HST image shown in Fig 2. There is a bimodal distribution of colours, with the blue clusters more centrally located (Carlson et al. 1998) and some are possibly associated with the high-velocity system. The majority of the stellar clusters appear red in colour, and are scattered uniformly around the galaxy. Clusters are visible up to the edge of the Gemini acquisition image, beyond 80 kpc from NGC 1275. Although there are brighter, clumpy structures within the line-emitting filaments, there does not appear to be any preferential spatial association of the star clusters with the filaments in either the Gemini or HST images (e.g. Figures 3, 4).

Figure 2 does, however, show a 1-arcminute-long chain of exceptionally blue star clusters that stretch from just north of the small cluster galaxy at RA 03:19:46.7, Dec 41:31:45.6 (J2000), down into the western edge of the intervening high-velocity system. This chain is an extension of the blue clusters noted by Conselice et al. (2001) in their Figure 8. It is absent from the Hα image of the low velocity system (Fig. 1) and from Hα images of the intervening high velocity system (Caulet et al. 1992). The only blue knot that coincides with Hα emission is marked by a white arrow in Fig. 2, it has a line-of-sight velocity of 5538 km s^{-1} which firmly places it
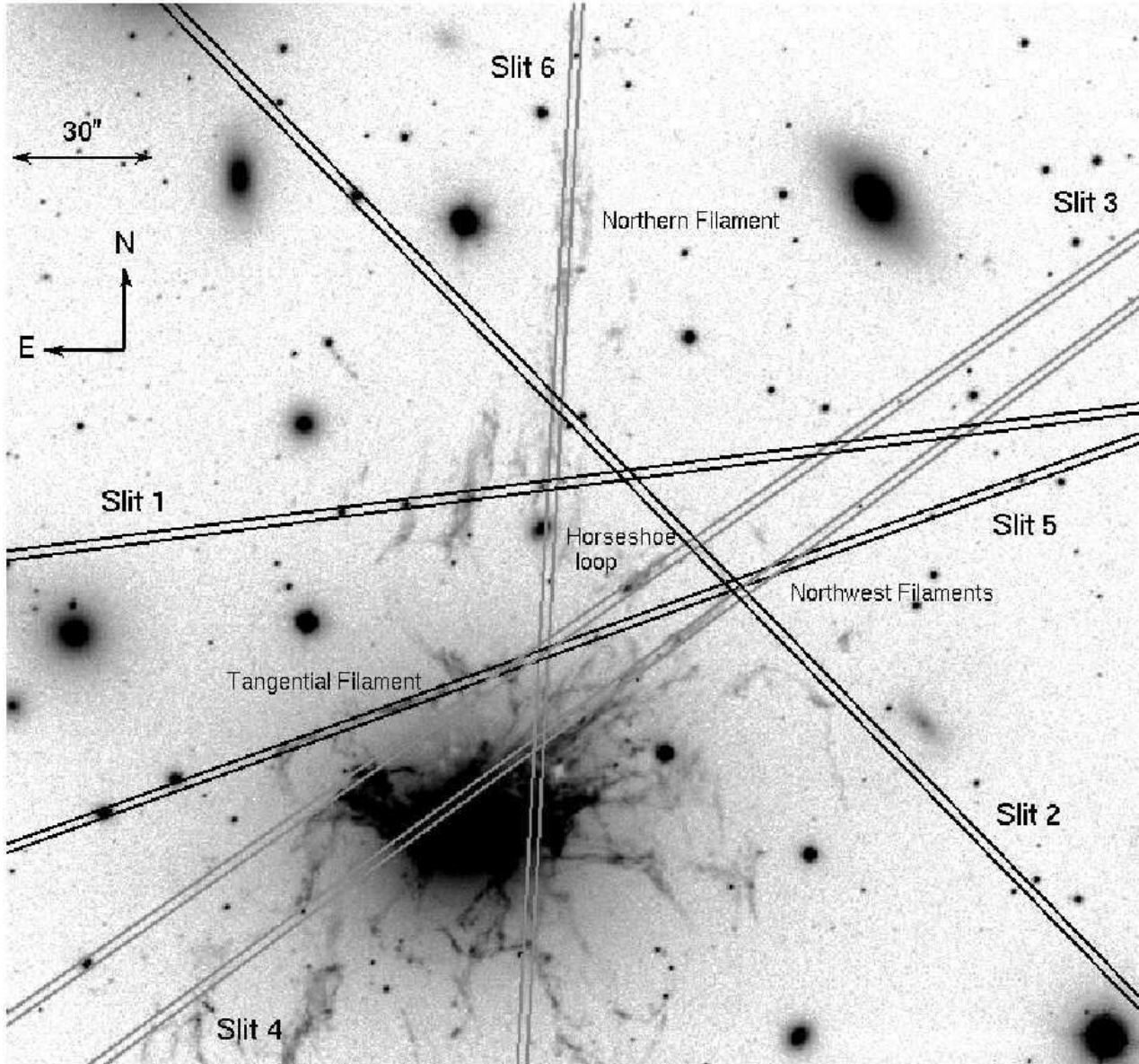
Figure 1. Position of the six longslit observations on the Hα nebula surrounding NGC 1275. The background image is taken from the data of Conselice et al. (2001)

within the low velocity system. The spatial connection and similarity in colour to the structures within the high-velocity system suggest that many of these blue star clusters may be associated with the disrupted foreground galaxy. The high-resolution HST image shows the Hα filaments themselves to be highly smooth (Figure 4) and continuous, consisting of several strands which are individually unresolved on scales of 0.25 arcsec (corresponding to 90 parsecs).

Excluding the central region where continuum from the galaxy is prominent, our spectra show signs of continuum only at 9 regions. Two of these regions exhibit no line emission so the continuum may have originated from stellar clusters which typically do not have Hα emission (Holtzman et al. 1992). The other 7 regions exhibited line emission with very similar line intensity ratios to regions without continuum and only one exhibited [OIII]λ5007 emission (see Figure 16 in section 7.3.1). The Hα luminosity from these continuum regions is fairly typical. Although the continuum

regions are distinct in the R-band acquisition image as stellar clusters, the HST images show that these bright knots are ubiquitous throughout the region stretching beyond the emission-line nebula. These are likely to be chance associations of alignment. It does not appear that the stellar clusters are formed or located within the filaments.

5 KINEMATICS OF THE NEBULA

The morphology of the filaments suggest they act as streamlines tracing the gas flow in the ICM. Therefore the Doppler shifts of the filaments may reveal the velocity field in the core of the cluster, near NGC 1275. The forces that could drive the flow of filaments are gravity (from NGC 1275), which would draw the filaments inwards, or the outward pull following a buoyantly rising radio/ghost bubble as proposed by Bohringer et al. (1995);
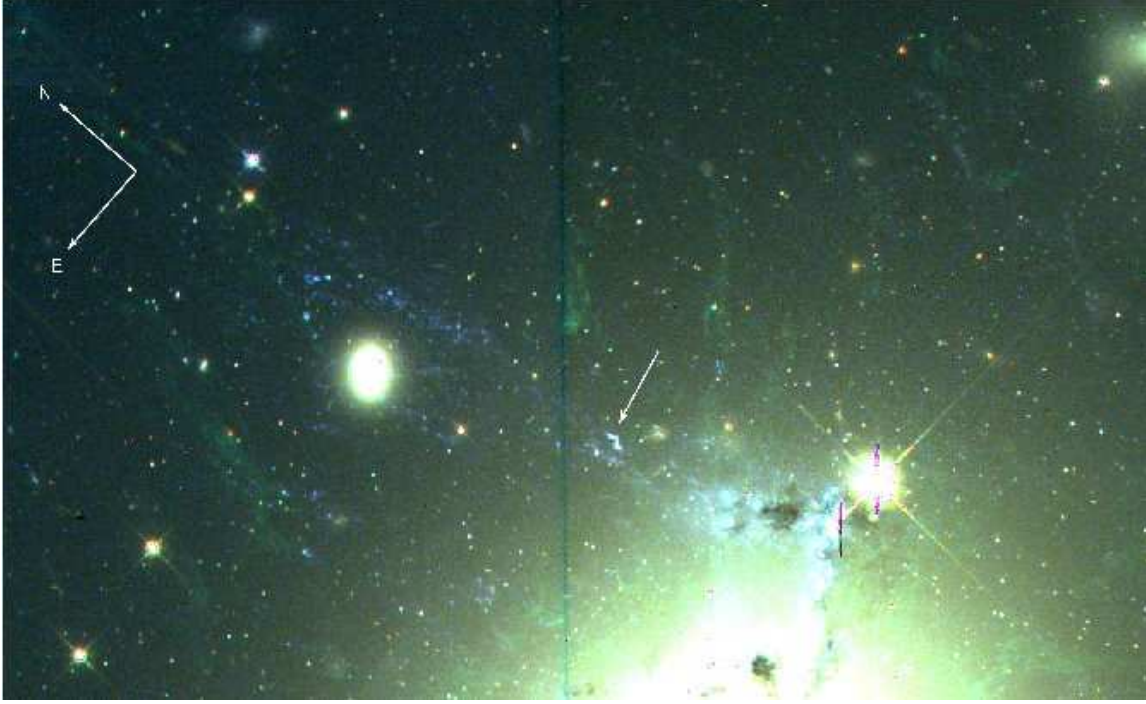
Figure 2. Combined colour image of the North and West environment of NGC 1275 as seen through the HST F450W (shown as blue), F702W (green) and F814W (red) broad-band filters. The F702W filter encompasses Hα+[NII] line emission at the redshift of NGC 1275. The image is 120 arcsec by 73 arcsec in size. The Northwest and Northern filaments including the 'horseshoe' loop are visible. A 1-arcminute-long chain of blue stellar clusters runs from the top left (above the cluster galaxy) toward the bottom right where it meets the Western edge of the infalling galaxy (high-velocity system) near the bright star. The white arrow points to a region where the detected Hα emission is redshifted by $5538 \, \mathrm{km \, s^{-1}}$ placing it in the low-velocity system.
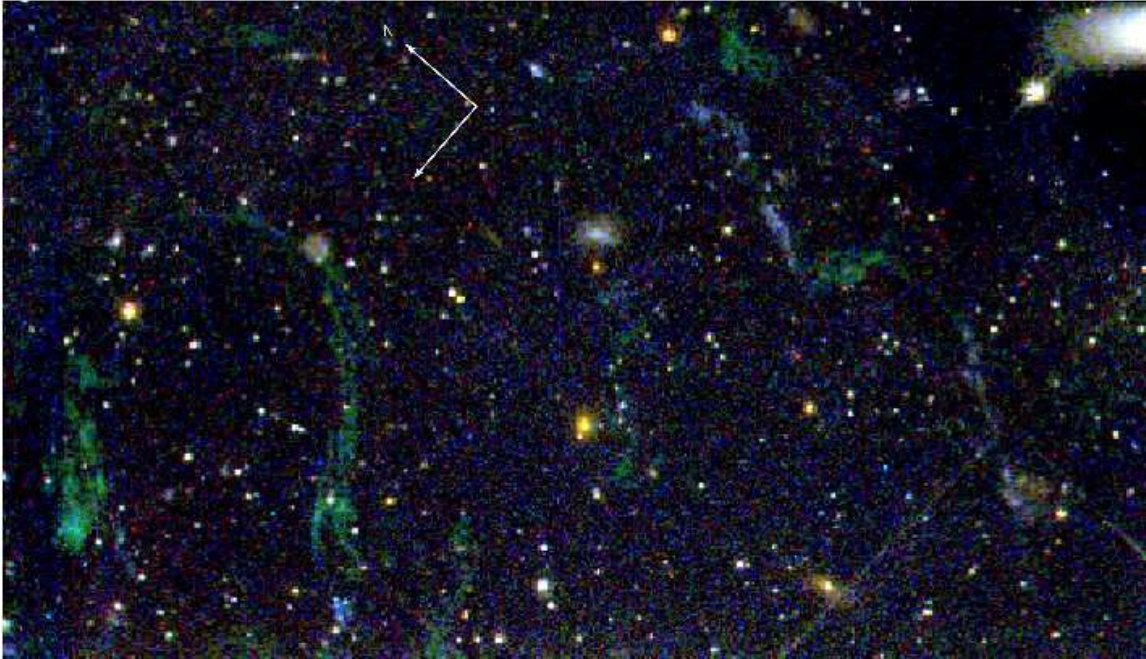

Figure 3. A zoom to the Northwest of the previous figures, showing detail of the loops in the region of the 'horseshoe' filament. The three colour images have each been unsharp-masked to remove the light from the underlying central galaxy. The image is 66 by 38 arcsec in size.
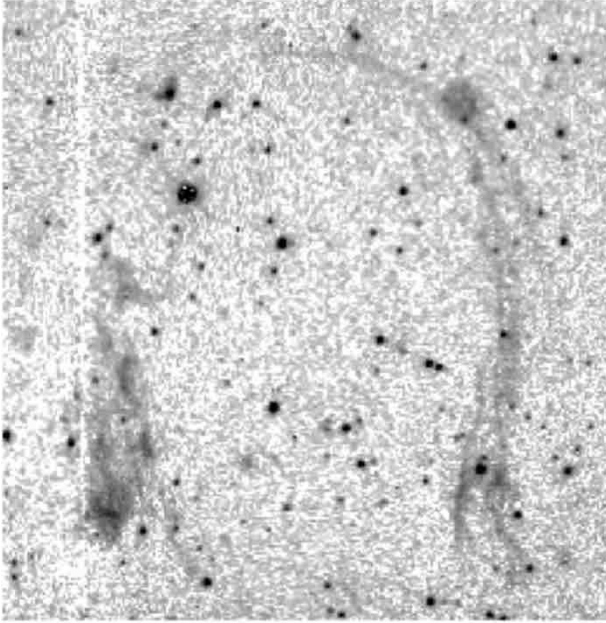
Figure 4. A detailed image of the Hα 'horseshoe' filament as seen through the HST F702W broad-band filter, showing the fine structure and smoothness of the individual strands. The image is 24 arcsec on a side, and has been unsharp-masked (i.e. it has had a highly smoothed version of itself subtracted) to remove the underlying gradient due to the light from the central galaxy continuum.

Churazov et al. (2001); Reynolds et al. (2005). A three dimensional flow pattern can differentiate between galactic outflow and inflow models, and thus constrain the origin of the filaments. The velocities are determined from binning the spatial dimension of the longslit spectra in bins of 4 pixels (0.58 arcsecond). All velocities presented are heliocentric and the line-of-sight zero point is defined as the velocity of NGC 1275, assumed to be 5265kms^{-1} (Ferruit et al. 1997). All distances referred to are projected distances.

5.1 Northern filament

The Northern filament is the dominant long ($\sim$60 kpc), thin (<1 kpc) structure stretching radially North-South, situated North of NGC 1275; slit 6 was positioned along this filament. The velocity structure of the Hα and [NII] lines is shown in Figure 5. The filament appears extremely radial for the majority of its length suggesting that the dominant direction of flow is also radial. As this filament is the only structure detected so far out from the galaxy it is extremely unlikely to be in projection with another filament, and therefore we assume it to be a single structure. It is improbable that we should be viewing an intrinsically-curved filament as a linear one, so we assume that it is intrinsically straight.

The filament has a kinematic North-South divide: the North displaying a velocity blueshift by up to -180km s^{-1}, whereas the South is erratically redshifted. The Northern half (above 37 kpc) is clumpy on scales of up to 5 kpc in length. Each clump exhibits smooth velocity gradients, although there are velocity discontinuities between the clumps. It is possible that some of the velocity could be due to the filament twisting as it falls (note the helical nature of the lower parts of the filament, Fig. 5). The Southern part of

this filament is split into two vertical segments: slit 6 covers only the western dimmer segment, whilst slits 1 and 2 slice across both. The Western segment is very thin and redshifted. The Eastern segment appears thicker and clumpier, and slit 2 shows that the emission is blueshifted. Slit 1 shows that the very bottom of the Eastern segment is redshifted.

The kinematic North-south divide indicates the lower part of the filament is moving in the opposite direction to the upper part of the filament: the filament is either being stretched or is collapsing, depending on whether it is orientated toward or away from the observer. Half of this filament must be falling into the galaxy, and the other half must be flowing away from the galaxy. Thus we can immediately rule out a model in which the filaments are smoothly falling onto the galaxy below. The Doppler shifts alone do not enable us to determine which end of the filament is inflowing or outflowing since we then need to know the inclination. However, as part of the filament must be flowing away from the galaxy, there must be a mechanism for drawing gas away from the galaxy.

We note that the Southern end of the three radial Northern filaments coincides with a shock front seen in the X-ray images (Fabian et al. 2003a). This front is due to the formation of the inner Northern bubble around the radio source which is a cyclical process taking place every 10^7 yr or so (as indicated by the presence of the outer ghost bubbles). If an expanding shock front destroys the emission-line filaments, then the lower part of the Northern filaments must previously have been at a larger radial distance in order to have survived the shock emitted from the Northwest ghost bubble when it was forming. Therefore the lower half of the Northern filament is probably moving inward, whilst the upper segment is moving outward, i.e. the filament is likely to be stretching.

There is a depression in the thermal pressure just above the Northern filament (Fabian et al. 2005), that could be a remnant of a ghost bubble that has buoyantly risen from the central region. We can now interpret the filament in the context of the rising bubble models of Bohringer et al. (1995); Churazov et al. (2001); Fabian et al. (2003b); Reynolds et al. (2005). The radial filament morphology traces the primary direction of flow therefore it acts as a streamline. Part of the filament is flowing away from the galaxy due to the uplift caused by the ghost bubble's buoyant rise through the ICM, whilst the other half has been overcome by the galaxy's gravity and is now flowing back. The pull from the bubbles competes with gravity.

For a total filament length of 25 kpc and a range in velocity of 400km s^{-1} the dispersion time is 6×10^7 years; if the filament is at a small angle from the plane of the sky (as is likely due to its large projected length) the velocity range may be much larger, reducing the dispersion time.

5.2 Northwest filaments and 'horseshoe' feature

To the Northwest of the galaxy lies an array of radial filaments, one of which extends 30 kpc from the nucleus and ends in a curved loop that Conselice et al. (2001) refer to as the 'horseshoe' (detail in Fig. 4). The loop is positioned underneath a ghost bubble visible as a prominent depression in the X-ray image (Fabian et al. 2003a).

The morphology of these filaments has previously been noted to resemble the flow underneath an air bubble rising in water (Fabian et al. 2003b). Figure 6 details the line-of-sight velocities of these filaments. The long radial filament (Western part of the 'horseshoe' loop) begins with a redshifted line-of-sight velocity of 95kms^{-1} which remains fairly constant for 5 kpc until the line emission shifts Southwest beyond the slit for 3 kpc, to reappear at a
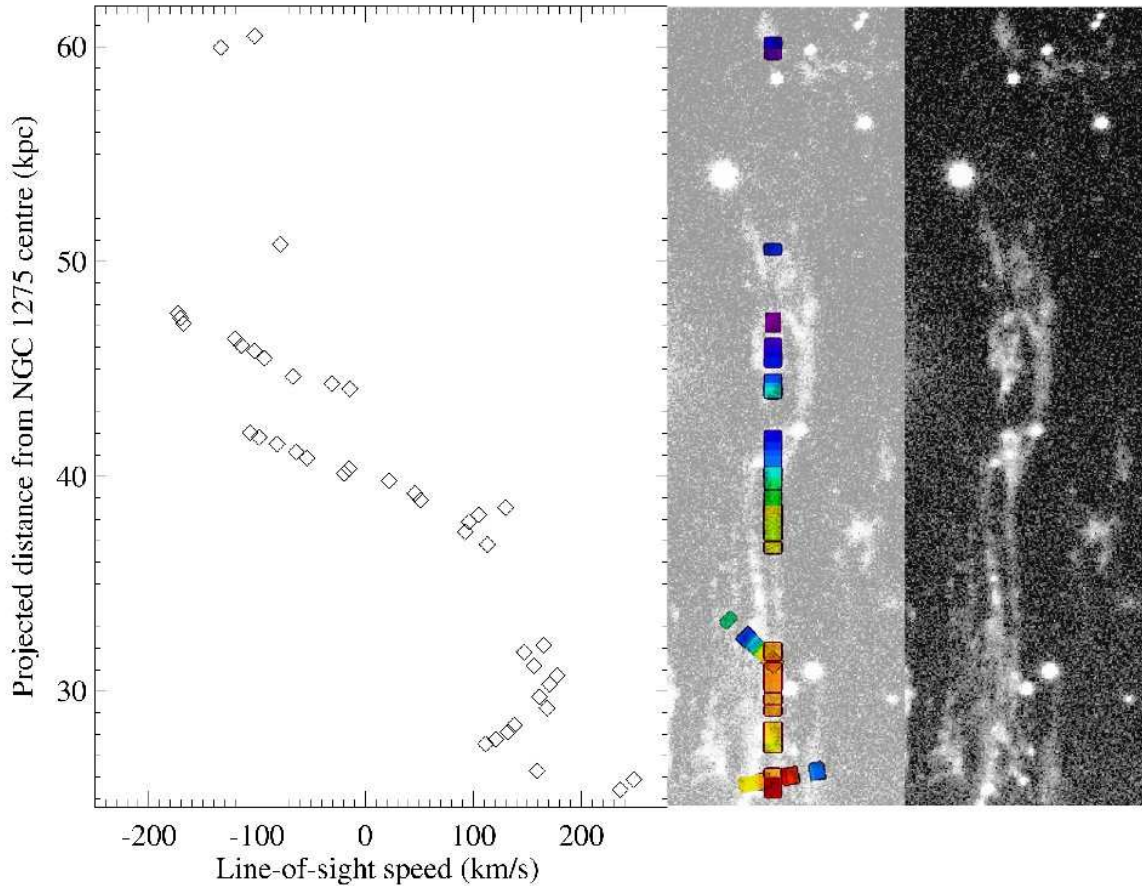
Figure 5. Line-of-sight velocities of the Northern filaments. Purple-blue indicate blueshifted emission, yellow-red indicate redshifted emission, whilst green has zero velocity relative to the central galaxy. Velocities from slit 1 (bottom) and slit 2 (top) which cut across the Northern filament are displayed in the image but not shown in graph. Background images are from the data of Conselice et al. (2001).

distance of 18 kpc from the galaxy with a velocity of $60 \, \mathrm{km s^{-1}}$. The difference of $35 \, \mathrm{km s^{-1}}$ between the two sides of this gap cannot be unambiguously attributed to a change in speed as a small change in orientation to the plane of our line of sight could also produce the observed velocity deviations.

From 18 kpc upward, this filament divides into two velocity structures before curving into the loop which starts at 22 kpc (see right panel of Fig. 6). These velocity structures have smooth gradients with no small scale random deviations in excess of the error (1-$10 \, \mathrm{km s^{-1}}$ depending on the line strength). The low velocities, morphological structure of the filaments, and the spherical cap appearance of the ghost bubble, indicate the filament may be close to being in the plane of the sky.

The curved part of the 'horseshoe' starts at a projected distance of 22 kpc from the nucleus where the velocity increases rapidly to $200 \, \mathrm{km s^{-1}}$, and remains steady over 4 kpc. The top of the loop has the highest velocity, peaking at $300 \, \mathrm{km s^{-1}}$, then slowing down to $200 \, \mathrm{km s^{-1}}$ as the loop turns over. On the short side of the loop the emission is still redshifted but the velocity dies to $60 \, \mathrm{km s^{-1}}$ in under 1 kpc and remains steady for the rest of the loop. Above the loop is gas with a blueshifted line-of-sight velocity of $-230 \mathrm{km s^{-1}}$, a jump in velocity space of more than $480 \mathrm{km s^{-1}}$ over a projected distance of 3 kpc. Further above the central axis of the bubble slit 5 cuts across some dim emission which is also blueshifted. The gas in the loop and above the loop surrounds the

ghost bubble suggesting the gas above the loop is part of the same structure as that in the loop and is not just a projection effect.

The flow pattern qualitatively matches the simulations of Reynolds et al. (2005) of a bubble rising through a viscous ICM: gas above the bubble flows in the opposite direction to the gas below the bubble, and the largest velocities occur near the central axis and close to the bubble. If the flow of cool gas starts from the galaxy, to stream up the long straight side, around the curve and down the short straight side, we would expect the material in the short straight side to be flowing in the opposite direction to the long straight side, similar to that in an eddy, with blueshifted emission underneath the bubble. Indeed the emission from the short straight side is blueshifted relative to the rest of the loop: at a height of 25 kpc from the nucleus, one side of the loop has a velocity of $200 \, \mathrm{km s^{-1}}$ whereas the other side is at $60 \, \mathrm{km s^{-1}}$.

The agreement of the velocities, morphology and the clear ghost bubble visible in the X-ray images of the Perseus cluster (Fabian et al. 2003a), suggest the most likely dynamical model is one in which the loop and radial filament is flowing out of the galaxy, with the filament slightly orientated away from us. As the bubble has risen (possibly with velocities of $700 \mathrm{km s^{-1}}$ Fabian et al. 2003b), it has dragged up cool material from the galaxy producing the filamentary structure we observe.
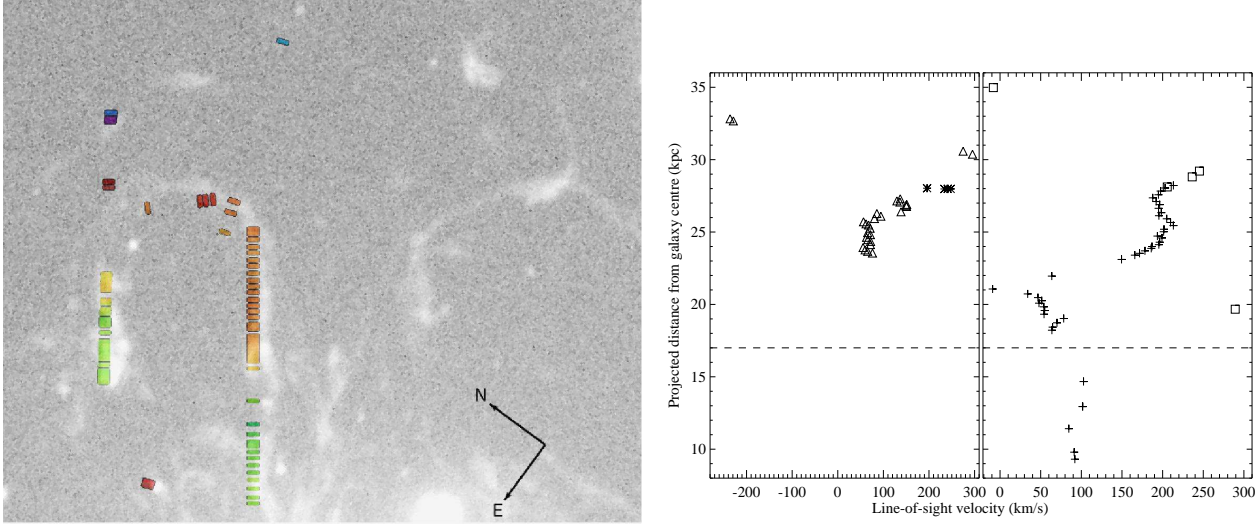
Figure 6. Left: Line-of-sight velocities along the 'horseshoe' loop. Positive velocities are red, blue indicates negative velocities relative to galaxy. Right: Left panel shows velocities on the short straight of the loop covered by slit 3 (triangles) and along the top of the loop, covered by slit 2 (stars). Right panel shows data from the long straight on the right-hand side covered by slit 4 (crosses) and data from slit 5 that crossed through the loop (squares). Only data above dashed line is presented in image. Background image is from the data of (Conselice et al. 2001).
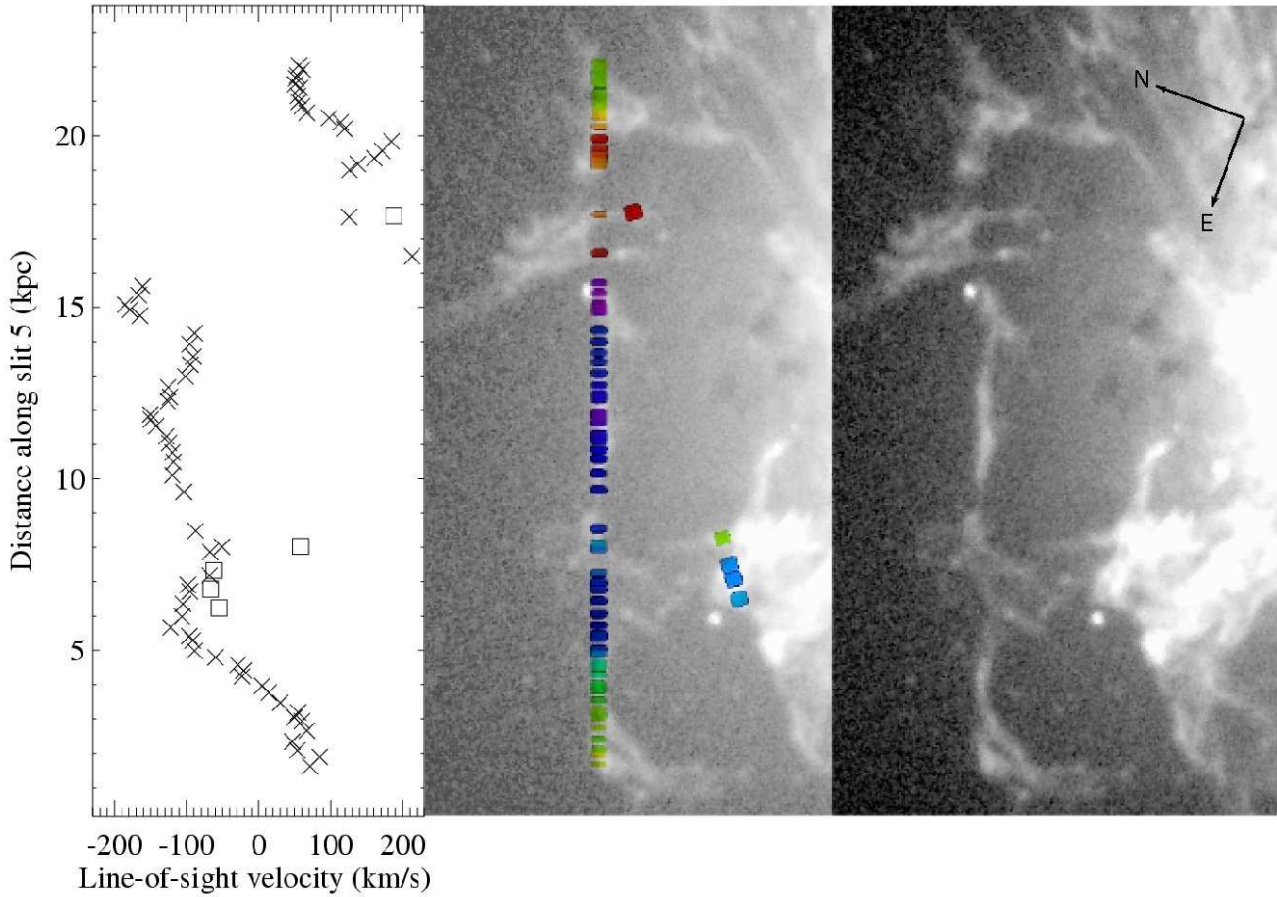
Figure 7. Line-of-sight velocities of the tangential filament running along the Northeast of NGC 1275. Purple-blue indicate blueshifted emission, yellow-red is redshifted emission and green has zero velocity relative to the central galaxy. Data from slit 5 is presented in the graph with crosses. Slit 3 also covered some nearby regions which have been marked by the square symbols. Luminous radial filaments extending from the galaxy to the tangential filament appear at the bottom right of the image. Background image is from the data of Conselice et al. (2001).

5.3 Tangential filament

Fig. 7 shows the line-of-sight velocities of the filament that appears to run tangentially along the North of the galaxy. Slit 3 also covered line emitting regions situated between the tangential filament and the galaxy whose velocities have been added into Figure 7 as square symbols.

The velocity structure along 14.5 kpc varies without large velocity jumps so the Eastern section of the filament appears to be a coherent structure. The emission is blueshifted to a similar velocity along $\sim$10 kpc of its length then smoothly decreases in speed at the most Eastern end. Small scale deviation from the large scale trends are seen in excess of the error ($\sim$1–10 km s^{-1} depending on the line intensity), suggesting some small scale random variations in velocity. Beyond 14.5 kpc the emission first jumps by –80 km s^{-1} in velocity then jumps again by almost +400 km s^{-1}. The Western section of this filament is not coherent in velocity space, and the morphology suggests that slit 5 is slicing across radial filaments that extend to the Northwest, in the same direction as the 'horseshoe' feature. The Eastern section is a puzzling structure since it is tangential, unlike the majority of the filaments. Interpretation of this region is complicated by the presence of the Northern radio lobe and complex X-ray emission.

6   FILAMENT LINE-WIDTHS AND VELOCITIES

The FWHM (full width at half maximum) of the instrumental profile is 85 km s^{-1} (2.85 pixels) at Hα determined from nearby sky lines. Most of the material has FWHM line-widths of 50-160 km s^{-1} after correcting for the instrumental broadening (Fig. 8), much greater than the thermal width of hydrogen gas at 10,000 K ($\sim$20 km s^{-1}). If the filaments represent an inflow of gas as predicted by early models of cooling flows (Fabian et al. 1984) we would expect an anti-correlation between line-widths and radial distance from the nucleus and extremely large ($\sim$500–1000 km s^{-1}) central line-widths (Heckman et al. 1989). We observe a few points within 10 kpc that have large ($>$200 km s^{-1}) line-widths. It is within 10 kpc of the galactic centre that the density of the line-emitting filaments increases greatly and there are many regions where the spectra display double peaked lines indicating that the line-of-sight crosses at least two clumps of line-emitting material which have different kinematics. It is not necessary that these clumps be physically close, therefore they do not imply small-scale velocity deviations along a single filament as observed in slit 5. Examples of such regions are shown in Fig. 9, and were either resolved into two sets of lines or removed from the dataset if the result was ambiguous. However, it is likely that some of these central regions would have clumps with similar line-of-sight velocities and result in spectra with a single wide peak. Most regions with large line-widths also have a large Hα surface brightness (Fig. 8), therefore it is probable that the spectra from these inner regions are caused by filaments overlapping in the same line-of-sight with slightly different velocities. Beyond the inner 10 kpc, the line-widths are uniformly 2–8 times the thermal width of gas at 10,000 K. Some radially extending filaments exhibit similar line-widths along their whole length (see Fig. 14 in section 7). Therefore the line-widths provide no evidence to suggest the nebula flows into the galaxy.

No line-of-sight velocity greater than 350 km s^{-1} was detected. This work primarily probes the outer filaments, which are likely to have small angles from the plane of the sky due to their large projected distance from the galaxy, and therefore are not expected to have large line-of-sight velocities. Cigan et al. (2004)
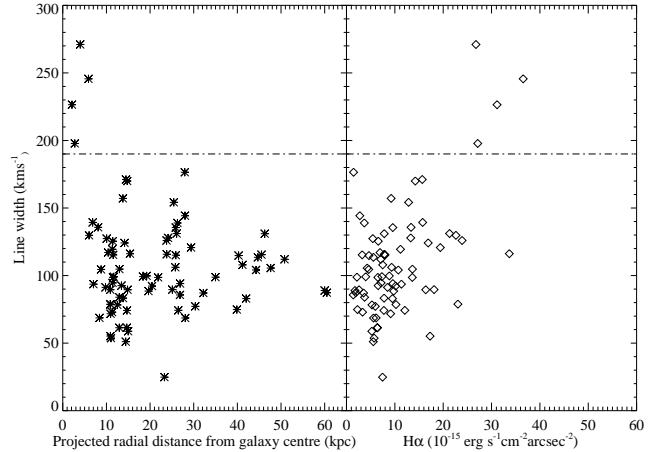

Figure 8. Left: Radial projection of emission line widths in km s^{-1} based on the Hα and [N II] lines. **Right**: Line width verses Hα surface brightness. Most points with large line-widths ($>$200 km s^{-1}) are within the central few kpc and have large Hα surface brightness suggesting they may be overlapping filaments.
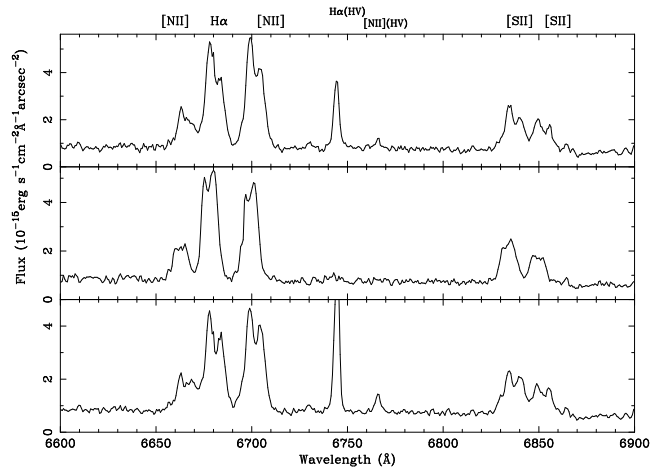

Figure 9. Examples of central clumps which show double-peaked line emission. These regions are all centrally located. HV denotes emission from the high-velocity system which lies infront of NGC 1275.

who probe the central regions as well as the outer filaments find no velocities greater than 450 km s^{-1}. In section 5.2 we argue that the 'horseshoe' feature and the Northwest filaments covered by slit 4 are very close to being in the plane of the sky. Therefore the observed line-of-sight velocity of 200 km s^{-1}, at the top of the 'horseshoe' loop could transform to a velocity much greater than 700 km s^{-1} (expected if tilted by a conservative 75° from the line-of-sight). This is far beyond what is observed in the rest of the dataset. It is possible that the two inner radio lobes have pushed or destroyed the filaments pointing toward our line-of-sight.

7   SPECTRAL FEATURES

Our data probe the outer nebula that extends beyond 10 kpc in detail for the first time. All intensity line ratios and line intensities are determined from binning the spatial dimension of the longslit spectra in bins of 6 pixels (0.87 arcsecond). A typical spectrum is shown in Fig. 11 and line intensity ratios are summarised in Table 2. All
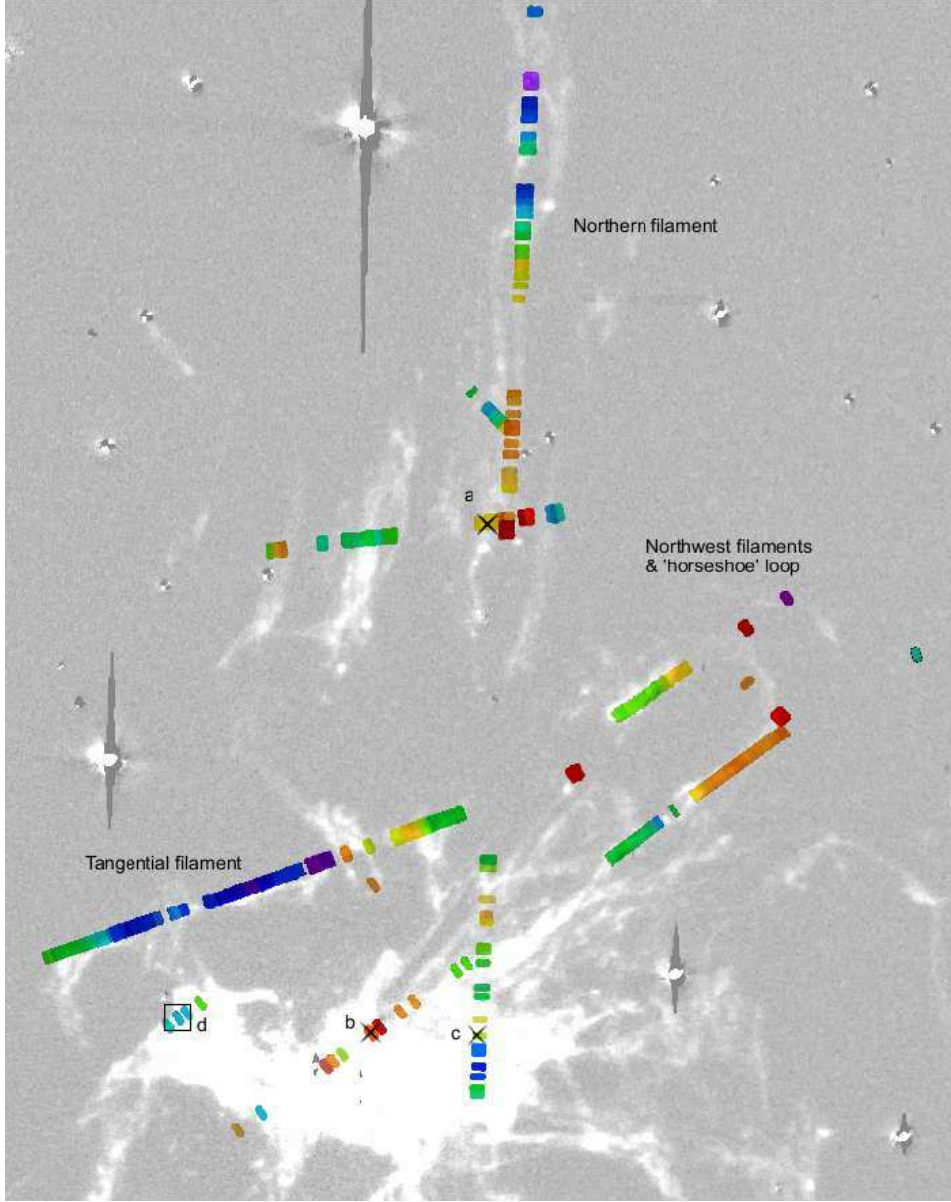
Figure 10. All velocities and regions from which spectra are shown in this work are marked. The region marked by a square and labelled **d** is where the typical spectrum from Fig. 11 is extracted. The regions marked by a cross and labelled **a**, **b** and **c** are the regions where [OIII]λ5007 is detected; the spectra are displayed in section 7.3.1. The regions which exhibit double peaked emission come from the central areas covered by slits 4 and 6 and are located near the labels **b** and **c**. The background image comes from the data of Conselice et al. (2001).

	Hα surface brightness (10^{-15} erg cm^{-2} s^{-1} arcsec^{-2})	[NII]λ6584/ Hα	[SII]λ6716/ Hα	[OI]λ6300/Hα	[SII]λ6716/ [SII]λ6731	Hα/Hβ	HeIλ5876/Hβ	[NI]λ5199/Hβ
Typical values	<15	0.3-1.5	0.14-0.54	0.1-0.3	1.4	3.5-7	0.2-0.3	0.4

Table 2. Range of typical line intensity ratios within the extended nebula

spectra exhibit low-excitation features: high [NII], [OI] and [SII] compared to Hα. The appearance of strong [OI] and [SII] confirm we are observing an ionization bound nebula as these species are observed from the partially ionized region beyond the classical HII region. There is a whole body of material on the optical line ratios from the central regions of this object and the reader is referred to

Kent & Sargent (1979); Heckman et al. (1989); Sabra et al. (2000); Conselice et al. (2001) and references therein. The low-ionization line emission extends from the central regions to the outer filaments. In the following sections we concentrate on the features illuminated by the study of the outer filaments. The Hα intensities range between 2–57$\times 10^{-15}$ erg cm^{-2} s^{-1} arcsec^{-2}, with the ma-
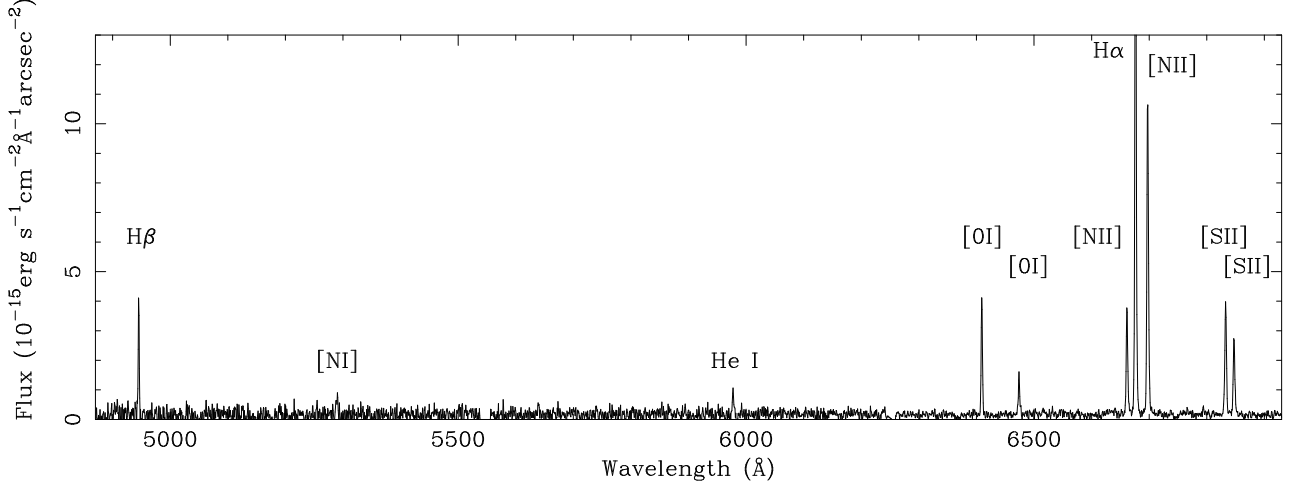
Figure 11. A typical spectrum showing the (low-velocity system) redshifted lines of [OI], [NII], Hα, Hβ, and [SII]. HeI and [NI] only appear in very luminous regions. The full strength of Hα is not shown.
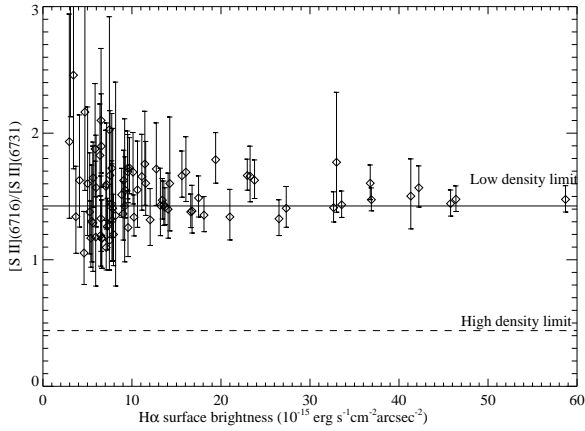

Figure 12. [SII]$\lambda 6716$/[SII]$\lambda 6731$ shows the gas is below the low density limit of 10^2cm^{-3}

Figure 13. [NII]$\lambda 6584$/Hα as a function of projected distance from the galactic centre. Data from slit 1 (squares), slit2 (stars), slit3 (triangles), slit 4 (crosses) and slit 6 (diamonds). 1σ error bars from error of line-fitting.

jority less than $15 \times 10^{-15} \text{erg cm}^{-2} \text{s}^{-1} \text{arcsec}^{-2}$. [NII]$\lambda 6584$/H$\alpha$ ratios tend to be higher near the nucleus. The line intensity ratio [SII]$\lambda 6716$/[SII]$\lambda 6731$ shown in Fig. 12 confirms the gas is in the low density limit, therefore is less than 10^2cm^{-3} (Osterbrock 1989), which agrees with measurements based on Hα surface brightness indicating the electron density is greater than 10cm^{-3} (Conselice et al. 2001).

7.1 Radial variation in emission-line ratios

The outer radial filaments to the North and Northwest show a clear correlation between the [NII]$\lambda 6584$/Hα intensity ratio and projected distance from the central galaxy. Fig. 13 shows the variation of [NII]$\lambda 6584$/ Hα along slits 1,2,3,4 and 6, which covers the 30 kpc radial filament that extends from the galaxy to the 'horseshoe' feature and the Northern filaments. Data from slit 5, the Eastern regions covered by slit 3, and the lower 15 kpc section covered by slit 6 were not included as the nebula morphology suggests these regions cut across many radial filaments (Fig. 10), hence the projected distance may not be a good approximation to the actual distance. Line-emitting regions within 4 kpc of the nucleus covered by
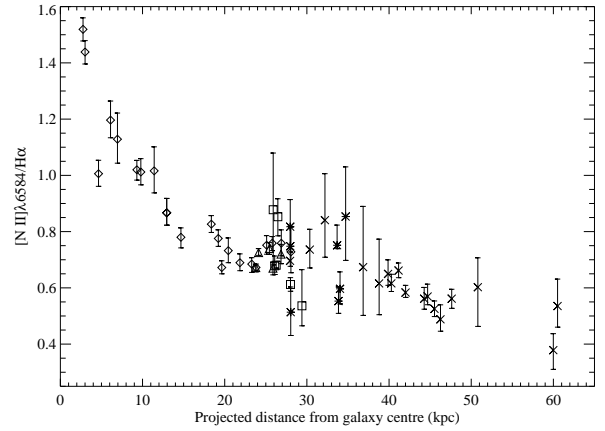
slit 4 have been removed from the dataset as the large line-widths and Hα luminosity (Fig. 14) suggest these sections are overlapping filaments. A clear radial gradient in the [NII]$\lambda 6584$/ Hα is observed. The slope is steeper up to 30 kpc than between 30–60 kpc which may be due to a projection effect. The Northwest filaments may have a larger inclination from the plane of the sky than the Northern filaments, therefore the projected distances below 30 kpc may correspond to a larger true distance compared to the datapoints from the Northern filaments which lie between 30–60 kpc. Such a gradient has also been observed in M87, the central galaxy of the Virgo cluster (Sarzi, M; private communication).

The Hα surface brightness remains constant along the filaments (Fig. 14), which rules out a central ionizing source which would produce a gradient in the Hα luminosity (Johnstone & Fabian 1988). If the filaments were excited by shocks we would observe a gradient in the line-width as well as in the [NII]$\lambda 6584$/Hα intensity ratio. Models of fast shocks by Dopita & Sutherland (1996) imply a range of FWHM of Hα between 150–300 km s^{-1} should be observed, therefore our data rule out fast shocks, but do not rule out shocks of moderate speed as
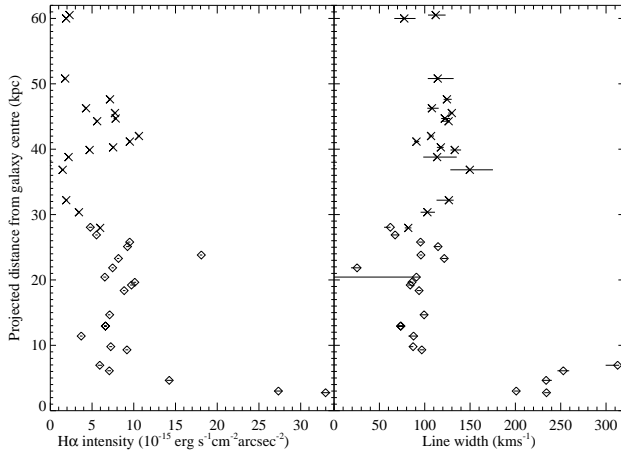
Figure 14. Line-width and Hα intensity shown as a function of distance from the galactic centre. Data taken from slit 4 (crosses) and slit 6 (diamonds). 1σ error bars from error of line-fitting.
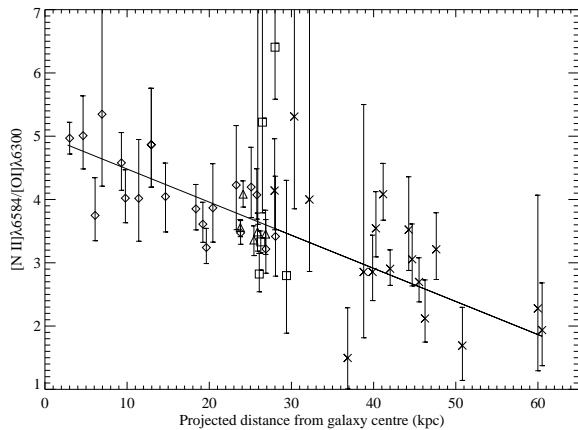

Figure 15. Data from slit 1 (squares), slit2 (stars), slit3 (triangles), slit 4 (crosses) and slit 6 (diamonds) showing variation of [NII]λ6584/[OI]λ6300 with distance from nucleus. The [NII]λ6584 line intensity increases more than the [OI]λ6300 line intensity. Lines indicates best fit to the data. 1σ error bars from error of line-fitting.

modelling of Shull & McKee (1979) imply a very steep gradient between a FWHM of 70–130 km s^{-1} would be observed. Our data show a great deal of scatter.

[NII] emission is produced by collisional excitation with electrons so the intensity of the line is a measure of the heat within the gas. The Hα line intensity measures the ionization rate within the gas, so the increasing [NII]λ6584/Hα line intensity ratio may indicate that more heating per Hydrogen ionization occurs within the gas close to the galaxy compared with the gas further out. Collisional excitation can be more efficient in dense environments, so this gradient could mirror the pressure variation of the surrounding ICM. The soft X-ray filaments detected by Fabian et al. (2003b) spatially coincide with the optical filaments, indicating an energy exchange occurs between the two gas phases. The [NII]λ6584/Hα gradient may be a further symptom of the interaction between the warm optical gas and the hot ICM. Alternatively this trend may be attributed to an extra heating mechanism originating from the central parts of NGC 1275. Increasing [NII]λ6584/Hα and [SII]λ6717/Hα intensity ratios have been observed extend-

ing above the plane of the Milky Way and of other spiral galaxies (Miller & Veilleux 2003) and is attributed to an extra heating mechanism (Elwert & Dettmar 2005).

The [NII]λ6584/Hα ratio is also sensitive to variations in metallicity. An increase in the nitrogen abundance would increase the [NII]λ6584/Hα ratio, however, as oxygen is an efficient coolant, an increase in the oxygen abundance would decrease the gas temperature and reduce the [NII]λ6584/Hα ratio. Therefore the [NII]λ6584/Hα line intensity ratio is sensitive to the nitrogen/oxygen abundance in the nebula. Fig. 15 plots the [NII]λ6584/[OI]λ6300 ratio against projected distance for the same regions plotted in Fig. 13. A small radial variation may be present, however the errors are too large to be conclusive. How metallicity variations affect the [NII]λ6584/Hα or [NII]λ6584/[OI]λ6300 ratio depends on the excitation mechanism. Since both the metallicity and excitation source are currently unknown, we cannot determine whether the radial variation in line ratios is due to metallicity changes or an excitation process.

7.2 Hα/Hβ ratio

The Balmer decrement for the filaments of NGC 1275 is high, Kent & Sargent (1979) place the value at 4.77 which corresponds to E(B-V)=0.43 under the assumption of case B recombination theory. Our data of the extended filaments, that are distinct from the high-velocity system, also have a high Hα/Hβ ratio, ranging over 3–7. We find Hα/Hβ ∼ 3 for the high velocity system in agreement with 3.15 from Kent & Sargent (1979). Therefore the decrement is caused by a process occurring in the filaments themselves, such as the photoionization mechanism suggested by Donahue & Voit (1991), involving EUV and soft X-rays would naturally lead to high Hα/Hβ ratios, or a great deal of dust either within the filaments or between the infalling galaxy and the low-velocity filamentary nebula. There is clearly a lot of dust associated with the high-velocity system as it appears in absorption in HST and X-ray images (Gillmon et al. 2004), however it is confined to the Northwest of NGC 1275. The dynamical model we present in section 5 implies the filaments are drawn out of the galaxy, therefore it is possible that the filaments are dusty. By contrast, if the filaments had condensed out of the ICM we would not expect them to immediately contain dust (Fabian et al. 1984).

7.3 Faint line-emission

7.3.1 [OIII] line-emission

The [OIII]λ4959 and λ5007 emission lines are not detected in most of the longslit spectra in agreement with observations of Meaburn et al. (1989). These lines are typically found in both high and low excitation spectra, and are commonly produced by hot stars, planetary nebulae, and active galactic nuclei. Studies of the inner nebula often detected [OIII]λ4959, λ5007 emission (e.g. Kent & Sargent 1979; Sabra et al. 2000). Since oxygen is clearly present throughout the whole nebula given the strong [OI]λ6300 emission line, it is probable that there is an additional excitation mechanism acting on the inner nebula which produces the [OIII]λ4959, λ5007 line-emission. The ionization mechanism in the outer nebula may not be hard enough to produce O^{++} which requires 54.93eV (similar to HeII which has not been detected in the NGC 1275 nebula). It is unlikely that the lack of [OIII]λ4959, λ5007 emission is due to a very high oxygen abundance in the
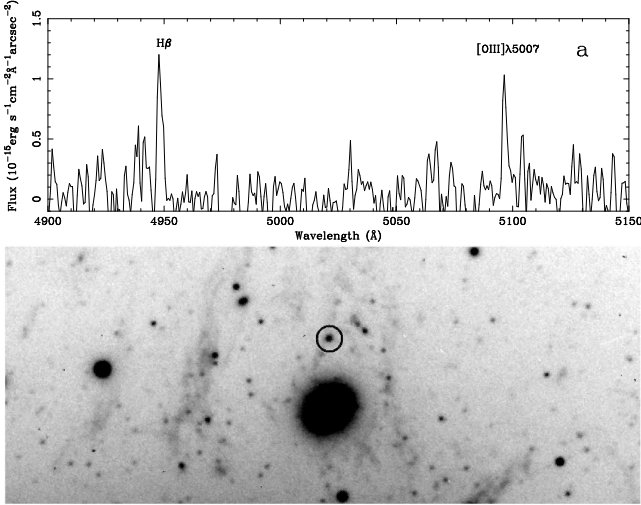
Figure 16. Spectrum of highlighted region showing clear [OIII] line. Black circle highlights a bright knot from which the [OIII] is detected.

Figure 17. Spectra of complex regions showing [OIII] lines. HV and LV denotes the high-velocity system and the low-velocity system respectively. The high-velocity system is an infalling galaxy infront of NGC 1275. The low-velocity system is the filamentary nebula surrounding NGC 1275.

	[OIII]λ5007/ Hβ	[NII]λ6584/Hα	[SII]λ6716/ [SII]λ6731	Hα surface brightness
a	0.78	0.61	1.32	12.0
b	3.5	1.44	1.41	27.3
c	0.61	0.87	1.41	32.7

Table 3. Line ratios of regions in which [OIII] 5007Å emission is detected. Hα surface brightness in units of (10^{-15} erg cm^{-2} s^{-1} arcsec^{-2}).

outer nebula compared to the inner nebula. A high oxygen abundance would cool the nebula through far-infrared lines at 52μm and 88μm which would result in reducing the optical [OIII] emission. It is even more improbable that the [OIII] lines are suppressed by collisional de-excitation which starts at a density of 10^6cm^{-3}, as the density measured from the [SII] lines is below this value by at least 3 orders of magnitude.

[OIII]λ5007 emission is detected in only three regions. The clearest detection occurs in slit 1 in the region marked by a circle in Fig. 16 with [OIII]λ5007/Hβ=0.78. This region also has continuum emission although all other features of the spectrum are fairly typical of the rest of the filaments (see Table 3 for details).

The other two spectra which have [OIII] lines are complex as both lie close to the galaxy centre and overlap the high-velocity system (Fig. 17). The [OIII]λ5007 line of the low-velocity system overlaps the [OIII]λ4959 line from the high-velocity system. This is particularly bad in spectrum b (Fig. 17) as the [OIII]λ5007 line from the high-velocity system is bright. Therefore the [OIII]λ5007 emission from the low-velocity system has been estimated from the λ4959 line using an intensity ratio of 2.98 (Storey & Zeippen 2000). Whilst the spectrum c has similar features to the clear detection in spectrum a, spectrum b has very different ratios. The spectral features are summarised in Table 3. It should be noted that spectra b and c also exhibit [NI]λ5199 emission which shall be discussed in the following section. If the ratio was set at 0.7 (as in spectrum a and b), the [OIII] 5007Å emission should be detectable in the majority of the longslits, therefore these regions are an exception in comparison to the rest of the studied nebula.
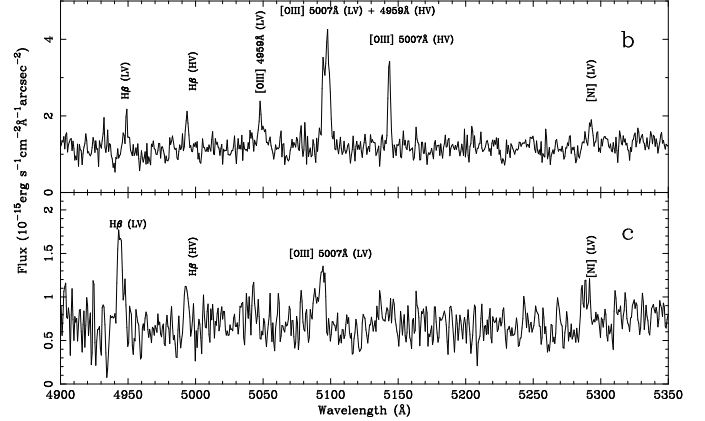
7.3.2 He I *and [NI] line-emission*

HeIλ5876 and [NI]λ5199 emission lines are commonly detected in the NGC 1275 nebula where the Hα surface brightness exceeds 30×10^{-15} erg cm^{-2} s^{-1} arcsec^{-2}. [NI] was only detected within 8 kpc of the nucleus, but there was one detection of HeI at a distance of 24 kpc from the nucleus, in the tip of the horseshoe loop. In total [NI] was detected in 7 regions whilst HeI was detected in 5 regions; only the region at the tip of the horseshoe loop had detectable HeI yet no clear [NI]. Given the low HeI/Hβ and [NI]/Hβ ratios of $\sim$0.25 and $\sim$0.4 respectively, it is possible that all the filaments emit through these lines, but the signal-to-noise of the observations is not high enough to detect them. The combination of [OI], [NI] and HeI emission suggests that the filaments have a layered structure such as observed in the Crab nebula (Sankrit et al. 1998). Warm molecular gas has been found at the same location as the filaments (Hatch et al. 2005) which implies there is a cool (2000 K) component associated with the ionized gas.

8 CONCLUSION

The kinematic data presented in section 5 rules out any dynamical models of purely infalling filaments. The low velocities and line-widths presented here argue strongly against inflow, as one would expect both these parameters to rise sharply toward the centre of the nebula (Heckman et al. 1989; Donahue & Voit 1991). The most conclusive evidence lies in the velocity structure of the Northern and Northwest filaments. The lower half of the Northern filament is redshifted,whilst the upper section is blueshifted, thus the upper section of the filament is moving in the opposite direction to the material below: part of the filament is flowing away from the galaxy, whilst the other part is flowing into the galaxy. In order to explain the outflow we appeal to the models of Bohringer et al. (1995); Churazov et al. (2001) and Fabian et al. (2003b) in which the radio emitting plasma from the AGN forms bubbles in the ICM, which detach to become buoyant and rise, dragging cool material from the galaxy below. The Northwest filaments lie directly underneath a ghost bubble (Fabian et al. 2003b). In addition to the morphological resemblance noted by Fabian et al. (2003b), the kinematic signature of these filaments matches simulations of gas flow under a buoyantly rising bubble (Reynolds et al. 2005), including

details such as gas above the bubble moving in the opposite direction to the filaments below.

The data suggests the filaments are outflowing and therefore their origins lie within the galaxy. NGC 1275 contains a large reservoir of cold molecular gas (Krabbe et al. 2000; Donahue et al. 2000) that can fuel these filaments. As we observe part of the Northern filament falling back into the galaxy it is possible that the fate of all filaments lie in an eventual return to the galaxy. However, if the filament falls back in segments as observed in the Northern filament, this would stretch and possible narrow the filament, making them more susceptible to evaporation by the ICM. The detection of [OI] and [NI] indicates the presence of warm atomic hydrogen, and warm molecular hydrogen has been found in the outer filaments (Hatch et al. 2005). It is possible the filaments holds a significant amount of cooler, so-far undetected gas. In the manner proposed above, the central galaxy can efficiently lose mass and pollute the ICM with metals.

We report a radial variation of the [NII]λ6584/Hα ratio, indicating either progressive hardening of the excitation mechanism close to NGC 1275, or a variation in the nitrogen/oxygen abundance.

Although NGC 1275 is surrounded by numerous stellar clusters, we have presented details of HST images which show there is no preferential association with the optical filaments (Figs. 3 and 4). As [OIII] emission (commonly found in HII regions) is also lacking in the filaments, it is unlikely to be powered by or the birthplace of hot young stars. The central region exhibits [OIII]λ5007 line emission, in contrast to the outer nebula, therefore an additional hard excitation source may be influential in the central region.

REFERENCES

Bohringer H., Nulsen P. E. J., Braun R., Fabian A. C., 1995, MNRAS, 274, L67

Boroson T. A., 1990, ApJ, 360, 465

Braine J., Wyrowski F., Radford S. J. E., Henkel C., Lesch H., 1995, A&A, 293, 315

Burbidge E. M., Burbidge G. R., 1965, ApJ, 142, 1351

Carlson M. N. et al., 1998, AJ, 115, 1778

Caulet A., Woodgate B. E., Brown L. W., Gull T. R., Hintzen P., Lowenthal J. D., Oliversen R. J., Ziegler M. M., 1992, ApJ, 388, 301

Churazov E., Brüggen M., Kaiser C. R., Böhringer H., Forman W., 2001, ApJ, 554, 261

Cigan P., Gallagher J., Zweibel E., 2004, American Astronomical Society Meeting Abstracts, 205,

Conselice C. J., Gallagher J. S., Wyse R. F. G., 2001, AJ, 122, 2281

Crawford C. S., Allen S. W., Ebeling H., Edge A. C., Fabian A. C., 1999, MNRAS, 306, 857

Crawford C. S., Fabian A. C., 1992, MNRAS, 259, 265

Donahue M., Mack J., Voit G. M., Sparks W., Elston R., Maloney P. R., 2000, ApJ, 545, 670

Donahue M., Voit G. M., 1991, ApJ, 381, 361

Dopita M. A., Sutherland R. S., 1996, ApJS, 102, 161

Edge A. C., Wilman R. J., Johnstone R. M., Crawford C. S., Fabian A. C., Allen S. W., 2002, MNRAS, 337, 49

Elwert T., Dettmar R.-J., 2005, in ASP Conf. Ser. 331: Extra-Planar Gas, p. 203

Fabian A. C., Nulsen P. E. J., Canizares C. R., 1984, Nature, 310, 733

Fabian A. C., Sanders J. S., Allen S. W., Crawford C. S., Iwasawa K., Johnstone R. M., Schmidt R. W., Taylor G. B., 2003a, MNRAS, 344, L43

Fabian A. C., Sanders J. S., Crawford C. S., Conselice C. J., Gallagher J. S., Wyse R. F. G., 2003b, MNRAS, 344, L48

Fabian A. C., Sanders J. S., Taylor G. B., Allen S. W., Crawford C. S., Johnstone R. M., Iwasawa K., 2005, preprint, astro-ph/051047

Ferruit P., Adam G., Binette L., Pecontal E., 1997, New Astronomy, 2, 345

Gillmon K., Sanders J. S., Fabian A. C., 2004, MNRAS, 348, 159

Hatch N. A., Crawford C. S., Fabian A. C., Johnstone R. M., 2005, MNRAS, 358, 765

Heckman T. M., Baum S. A., van Breugel W. J. M., McCarthy P., 1989, ApJ, 338, 48

Holtzman J. A. et al., 1992, AJ, 103, 691

Johnstone R. M., Fabian A. C., 1988, MNRAS, 233, 581

Kent S. M., Sargent W. L. W., 1979, ApJ, 230, 667

Krabbe A., Sams B. J., Genzel R., Thatte N., Prada F., 2000, A&A, 354, 439

Lynds R., 1970, ApJ, 159, L151

Meaburn J., Allan P. M., Clayton C. A., Marston A. P., Whitehead M. J., Pedlar A., 1989, A&A, 208, 17

Miller S. T., Veilleux S., 2003, ApJS, 148, 383

Minkowski R., 1957, in IAU Symp. 4: Radio astronomy, p. 107

Osterbrock D. E., 1989, Astrophysics of Gaseous Nebulae and Active Galactic Nuclei. University Science Books, p. 79

Reynolds C. S., McKernan B., Fabian A. C., Stone J. M., Vernaleo J. C., 2005, MNRAS, 357, 242

Sabra B. M., Shields J. C., Filippenko A. V., 2000, ApJ, 545, 157

Sanders J. S., Fabian A. C., Allen S. W., Schmidt R. W., 2004, MNRAS, 349, 952

Sankrit R. et al., 1998, ApJ, 504, 344

Schmidt R. W., Fabian A. C., Sanders J. S., 2002, MNRAS, 337, 71

Shull J. M., McKee C. F., 1979, ApJ, 227, 131

Storey P. J., Zeippen C. J., 2000, MNRAS, 312, 813

Tennant A. F., 1990, NASA Technical Memorandum 4301